PHYSICAL REVIEW D VOLUME 47, NUMBER 7 1 APRIL 1993

Order-α_s corrections to the differential cross section for the WH intermediate-mass Higgs-boson signal

J. Ohnemus[a,b] and W. J. Stirling[a,c]

[a]Department of Physics, University of Durham, Durham, DH1 3LE, England*

[b]Fermi National Accelerator Laboratory, P.O. Box 500, Batavia, Illinois 60510

[c]Department of Mathematical Sciences, University of Durham, Durham, DH1 3LE, England

(Received 16 October 1992)

The process $pp \to WH+X \to \ell\nu\gamma\gamma+X$ is calculated to order α_s. Results are given for differential cross sections at Superconducting Super Collider energies. The order-α_s corrections are found to be $\sim 10\%$ over most of the relevant kinematic region and are insensitive to cuts on the final-state particles.

PACS number(s): 13.85.Qk, 12.38.Bx, 14.80.Er, 14.80.Gk

I. INTRODUCTION

A standard model Higgs boson with mass in the intermediate range $M_W \lesssim M_H \lesssim 2M_Z$ is difficult to detect at a hadron collider. The production of a Higgs boson in association with a W-boson [1], followed by $H \to \gamma\gamma$ and $W \to \ell\nu$, provides a nearly background-free signal, although the expected number of events is small [2–8]. Thus it is important to calculate the cross section as accurately as possible. For example, a large "K-factor" from higher-order QCD corrections would have important implications on the collision energy and luminosity required for discovering the Higgs boson in this channel. In addition, calculating the cross section to next-to-leading order in QCD reduces the uncertainty associated with the choice of factorization scale in the parton distribution functions. The uncertainties in the parton distribution functions themselves will be further reduced when data from the DESY ep collider become available.

The total cross sections for $pp \to VH + X$ ($V = W^\pm$ or Z) to order α_s were first calculated by Han and Willenbrock in Ref. [9], where the total cross sections' dependence on the choice of factorization scale and parton distributions was discussed in detail. In this paper we calculate to order α_s the cross section for VH production with subsequent decays $V \to \ell_1\bar{\ell}_2$ and $H \to \gamma\gamma$ in a completely differential form so that differential distributions can be presented and acceptance cuts can be imposed on the decay products.

The next-to-leading-order (NLO) calculation presented here makes use of a combination of analytic and Monte Carlo integration methods. The same methods were used in Refs. [10–18] for the NLO calculations of ZZ, W^-W^+, $W^\pm Z$, $\gamma\gamma$, $W^\pm\gamma$, and $Z\gamma$ production, direct photon production, photoproduction, symmetric dihadron production, and single W production. In fact, most of the expressions for VH production can be obtained from the corresponding expressions for ZZ production by simply replacing the ZZ Born cross section with the VH Born cross section. The only exception to this rule is the finite virtual correction, which must be calculated anew. Thus only the final expressions for the NLO VH calculation will be given in this paper. Details on the derivations of these expressions can be found in Ref. [10].

The remainder of this paper is organized as follows. The formalism for the NLO calculation of VH production is described in Sec. II. Results are presented in Sec. III and summary remarks are given in Sec. IV.

II. NEXT-TO-LEADING-ORDER FORMALISM

The Monte Carlo formalism for NLO calculations has been described in detail in Refs. [10–18], so the discussion here will be brief. The basic idea is to isolate the soft and collinear singularities associated with the real emission subprocesses by partitioning phase space into soft, collinear, and finite regions. This is done by introducing theoretical soft and collinear cutoff parameters, δ_s and δ_c. Using dimensional regularization [19], the soft and collinear singularities are exposed as poles in ϵ (the number of space-time dimensions is $N = 4-2\epsilon$ with ϵ a small number). The infrared singularities from the soft and virtual contributions are then explicitly canceled while the collinear singularities are factorized and absorbed into the definition of the parton distribution functions. The remaining contributions are finite and can be evaluated in four dimensions. The Monte Carlo program thus generates n-body (for the Born and virtual contributions) and $(n+1)$-body (for the real emission contributions) final state events. The n-body and $(n+1)$-body contributions both depend on the cutoff parameters δ_s and δ_c; however, when these contributions are added together to form a suitably inclusive observable, all dependence on the cutoff parameters cancels.

For simplicity, the calculation is done for real H production. Since the Higgs boson is a scalar, it is trivial to

*Permanent address.

 ©1993 The American Physical Society

incorporate the decay $H \to \gamma\gamma$ into the calculation: simply multiply the cross section for real Higgs boson production by the branching ratio $B(H \to \gamma\gamma)$ and generate the photon four-vectors isotropically in the rest frame of the Higgs boson. The branching ratio $B(H \to \gamma\gamma)$ as a function of M_H can be found for example in Ref. [6]. In this paper we present results only for $M_H = 100$ GeV, for which $B(H \to \gamma\gamma) = 1.52 \times 10^{-3}$, assuming a heavy top quark.

A. Born process

The Feynman diagram for the Born process

$$q_1(p_1) + \bar{q}_2(p_2) \to VH \to \ell_1(p_3) + \bar{\ell}_2(p_4) + H(p_5)\,, \quad (1)$$

where $V = W^\pm$ or Z, is shown in Fig. 1. The squared matrix element, summed over final-state polarizations and initial-state spins, is

$$\left|\mathcal{M}^{\rm Born}\right|^2 = N_C\, e^4\, g_{VH}^2 \left|D(s_{12})\right|^2 \left|D(s_{34})\right|^2 \times \Big[G_{--}\, M_{--} + G_{-+}\, M_{-+}\Big]\,, \quad (2)$$

where N_C is the number of colors, e is the electromagnetic coupling constant ($e^2 = 4\pi\alpha$), g_{VH} is the weak-boson-to-Higgs-boson coupling,

$$g_{WH} = \frac{M_W\, e}{\sin\theta_{\rm w}}\,, \qquad g_{ZH} = \frac{M_Z\, e}{\sin\theta_{\rm w}\cos\theta_{\rm w}}\,, \quad (3)$$

and the function $D(x)$ is the weak boson propagator,

$$D(x) = \frac{1}{x - M_V^2 + i\Gamma_V M_V}\,. \quad (4)$$

The variables G_{--} and G_{-+} are combinations of weak-boson-to-fermion couplings,

$$G_{--} = \left|g_-^{q_2 V q_1}\right|^2 \left|g_-^{\ell_2 V \ell_1}\right|^2 + \left|g_+^{q_2 V q_1}\right|^2 \left|g_+^{\ell_2 V \ell_1}\right|^2\,, \quad (5)$$

$$G_{-+} = \left|g_-^{q_2 V q_1}\right|^2 \left|g_+^{\ell_2 V \ell_1}\right|^2 + \left|g_+^{q_2 V q_1}\right|^2 \left|g_-^{\ell_2 V \ell_1}\right|^2\,, \quad (6)$$

and the quantities M_{--} and M_{-+} are combinations of kinematic invariants,

$$M_{--} = 4\, t_{14}\, t_{23}\,, \qquad M_{-+} = 4\, t_{13}\, t_{24}\,. \quad (7)$$

The left- and right-handed weak-boson-to-fermion couplings are denoted by $g_\mp^{f_2 V f_1}$,

$$\begin{aligned} g_-^{f_2 W f_1} &= \left(g_-^{f_1 W f_2}\right)^* = \frac{U_{f_2 f_1}}{\sqrt{2}\sin\theta_{\rm w}}\,, \\ g_+^{f_2 W f_1} &= g_+^{f_1 W f_2} = 0\,, \\ g_-^{fZf} &= \frac{T_3^f}{\sin\theta_{\rm w}\cos\theta_{\rm w}} - Q_f \tan\theta_{\rm w}\,, \\ g_+^{fZf} &= -Q_f \tan\theta_{\rm w}\,, \end{aligned} \quad (8)$$

where Q_f and T_3^f denote the electric charge (in units of the proton charge e) and the third component of weak isospin of fermion f, θ_W is the weak mixing angle, and $U_{f_2 f_1}$ is the Cabibbo-Kobayashi-Maskawa quark mixing matrix. The parton-level kinematic invariants s_{ij} and t_{ij} are defined by

$$s_{ij} = (p_i + p_j)^2\,, \qquad t_{ij} = (p_i - p_j)^2\,. \quad (9)$$

The Born subprocess cross section is

$$d\hat{\sigma}^{\rm Born}(q_1\bar{q}_2 \to VH \to \ell_1\bar{\ell}_2 H) = \frac{1}{4}\,\frac{1}{9}\,\frac{1}{2s_{12}}\,|\mathcal{M}^{\rm Born}|^2\, d\Phi_n\,, \quad (10)$$

where the factors $\frac{1}{4}$ and $\frac{1}{9}$ are the spin average and color average, respectively, and $d\Phi_n$ is n-body phase space ($n = 3$ here). The Born cross section is obtained by convoluting the Born subprocess cross section with the parton densities and summing over the contributing partons,

$$\sigma^{\rm Born}(pp \to VH \to \ell_1\bar{\ell}_2 H) = \sum_{q_1,\,\bar{q}_2} \int d\hat{\sigma}^{\rm Born}(q_1\bar{q}_2 \to VH \to \ell_1\bar{\ell}_2 H) \times \Big[G_{q_1/p}(x_1, M^2)\, G_{\bar{q}_2/p}(x_2, M^2) + x_1 \leftrightarrow x_2\Big]\, dx_1 dx_2\,. \quad (11)$$

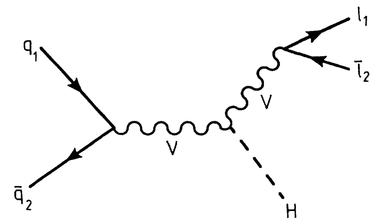

FIG. 1. Feynman diagrams for the Born subprocess $q_1\bar{q}_2 \to VH \to \ell_1\bar{\ell}_2 H$. The straight, wavy, curly, and dashed lines denote fermions, electroweak bosons, gluons, and Higgs bosons, respectively.

B. Next-to-leading-order cross section

When working to order α_s, one has to include the interference between the Born graphs of Fig. 1 and the virtual graphs shown in Fig. 2. In addition, one has to also include the real emission subprocess

$$q_1(p_1) + \bar{q}_2(p_2) \to VHg \to \ell_1(p_3) + \bar{\ell}_2(p_4) + H(p_5) + g(p_6) \quad (12)$$

(see Fig. 3). The NLO cross section, which consists of n-body and $(n+1)$-body contributions, can now be assembled from the pieces described in Ref. [10]. The n-body contribution is

$$\sigma_n^{\rm NLO}(pp \to VH \to \ell_1\bar{\ell}_2 H) = \sigma^{\rm HC} + \sum_{q_1,\bar{q}_2} \int dx_1\, dx_2 \left[G_{q_1/p}(x_1,M^2)\, G_{\bar{q}_2/p}(x_2,M^2)\, d\hat{\sigma}_n^{\rm NLO}(q_1\bar{q}_2 \to VH \to \ell_1\bar{\ell}_2 H) + (x_1 \leftrightarrow x_2) \right], \quad (13)$$

where the sum is over all contributing quark flavors and

$$d\hat{\sigma}_n^{\rm NLO}(q_1\bar{q}_2 \to VH \to \ell_1\bar{\ell}_2 H) = d\hat{\sigma}^{\rm Born}\left[1 + C_F \frac{\alpha_s}{2\pi} \left\{ \frac{2}{3}\pi^2 - 8 + 4\ln(\delta_s)^2 + [3 + 4\ln(\delta_s)] \ln\left(\frac{s_{12}}{M^2}\right) \right\} \right]. \quad (14)$$

The quantity $\sigma^{\rm HC}$ is the contribution from the hard collinear remnants. The real emission processes have hard collinear singularities when $t_{16} \to 0$ or $t_{26} \to 0$. These singularities must be factorized and absorbed into the initial-state parton distribution functions. After the factorization is performed, the contribution from the remnants of the hard collinear singularities has the form

$$\sigma^{\rm HC} = \sum_{q_1,\bar{q}_2} \int \frac{\alpha_s}{2\pi}\, d\hat{\sigma}^{\rm Born}(q_1\bar{q}_2 \to VH \to \ell_1\bar{\ell}_2 H)\, dx_1\, dx_2$$
$$\times \left[G_{q_1/p}(x_1,M^2) \int_{x_2}^{1-\delta_s} \frac{dz}{z} G_{\bar{q}_2/p}\left(\frac{x_2}{z},M^2\right) \tilde{P}_{qq}(z) + G_{q_1/p}(x_1,M^2) \int_{x_2}^{1} \frac{dz}{z} G_{g/p}\left(\frac{x_2}{z},M^2\right) \tilde{P}_{qg}(z) \right.$$
$$\left. + G_{\bar{q}_2/p}(x_2,M^2) \int_{x_1}^{1-\delta_s} \frac{dz}{z} G_{q_1/p}\left(\frac{x_1}{z},M^2\right) \tilde{P}_{qq}(z) + G_{\bar{q}_2/p}(x_2,M^2) \int_{x_1}^{1} \frac{dz}{z} G_{g/p}\left(\frac{x_1}{z},M^2\right) \tilde{P}_{qg}(z) \right], \quad (15)$$

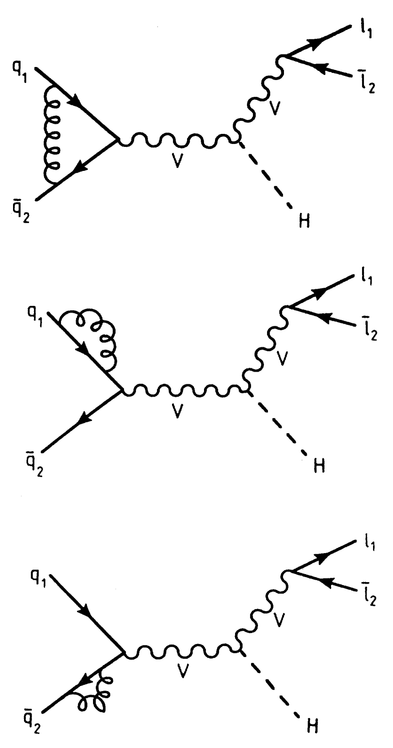

FIG. 2. Feynman diagrams for the virtual subprocess $q_1\bar{q}_2 \to VH \to \ell_1\bar{\ell}_2 H$.

where

$$\tilde{P}_{ij}(z) \equiv P_{ij}(z) \ln\left(\frac{1-z}{z}\,\delta_c\,\frac{s_{12}}{M^2}\right) - P'_{ij}(z). \quad (16)$$

The Altarelli-Parisi splitting functions in $N = 4$ dimen-

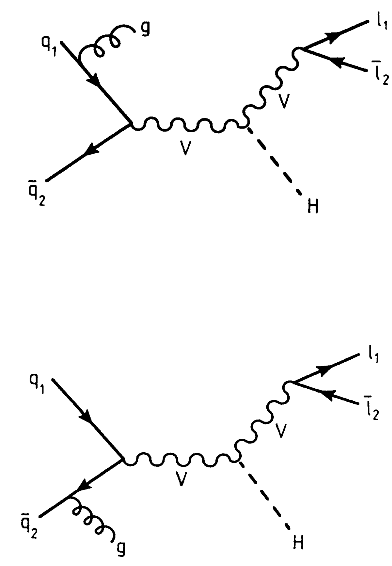

FIG. 3. Feynman diagrams for the real emission subprocess $q_1\bar{q}_2 \to VHg \to \ell_1\bar{\ell}_2 Hg$.

sions for $0 < z < 1$ are

$$P_{qq}(z) = C_F\left(\frac{1+z^2}{1-z}\right)\,, \quad P_{qg}(z) = \frac{1}{2}\left(z^2 + (1-z)^2\right)\,, \tag{17}$$

and the $P'_{ij}(z)$ functions are

$$P'_{qq}(z) = -C_F\,(1-z)\,, \quad P'_{qg}(z) = z\,(1-z)\,. \tag{18}$$

The parameter M^2 is the factorization scale, which must be specified in the process of factorizing the collinear singularity. Basically, it determines how much of the collinear term is absorbed into the various parton distributions.

Notice that all the singularities have been canceled or factorized; thus the expressions appearing here are finite and can be evaluated in four dimensions. Note also that Eqs. (14) and (16) are given in the modified minimal subtraction ($\overline{\rm MS}$) scheme [20]. Details on how to modify these equations for the deep-inelastic-scattering scheme can be found in Ref. [10].

The $(n+1)$-body contribution to the cross section is

$$\sigma_{n+1}(pp \to VH \to \ell_1\bar{\ell}_2 H + X) = \sum_{a,b,c}\int d\hat{\sigma}_{n+1}(ab \to VHc \to \ell_1\bar{\ell}_2 Hc) \times\left[G_{a/p}(x_1, M^2)\,G_{b/p}(x_2, M^2) + (x_1 \leftrightarrow x_2)\right]dx_1\,dx_2\,, \tag{19}$$

where the sum is over all partons contributing to the three subprocesses $q_1\bar{q}_2 \to VHg \to \ell_1\bar{\ell}_2 g$, $q_1 g \to VHq_2 \to \ell_1\bar{\ell}_2 q_2$, and $g\bar{q}_2 \to VH\bar{q}_1 \to \ell_1\bar{\ell}_2\bar{q}_1$. The cross section for the real emission subprocess is

$$d\hat{\sigma}_{n+1}(q_1\bar{q}_2 \to VHg \to \ell_1\bar{\ell}_2 g) = \frac{1}{4}\,A_C\,\frac{1}{2s_{12}}\,|\mathcal{M}^{\rm real}|^2\,d\Phi_{n+1}\,, \tag{20}$$

where the factors $\frac{1}{4}$ and A_C are the spin and color average, respectively. The squared matrix element, summed over final-state polarizations and initial-state spins, is

$$\left|\mathcal{M}^{\rm real}\right|^2 = \left(\frac{N_C^2-1}{2}\right) g_s^2\, e^4\, g_{VH}^2\, |D(p^2)|^2\,|D(s_{34})|^2 \times\left[G_{--}\,M_{--} + G_{-+}\,M_{-+}\right], \tag{21}$$

where g_s is the strong running coupling ($g_s^2 = 4\pi\alpha_s$), $p = p_1 + p_2 - p_6$, and

$$\begin{aligned} M_{--} = {} & \frac{8s_{12}}{t_{16}t_{26}}\left(2t_{14}t_{23} + t_{14}s_{36} + t_{23}s_{46}\right) \\ & + \frac{8}{t_{16}}\left(t_{14}t_{23} - t_{14}t_{13} + t_{23}s_{46}\right) \\ & + \frac{8}{t_{26}}\left(t_{14}t_{23} + t_{14}s_{36} - t_{23}t_{24}\right), \end{aligned} \tag{22}$$

$$M_{-+} = M_{--}(3 \leftrightarrow 4)\,. \tag{23}$$

The squared amplitudes for the subprocesses $q_1 g \to VHq_2 \to \ell_1\bar{\ell}_2 q_2$ and $g\bar{q}_2 \to VH\bar{q}_1 \to \ell_1\bar{\ell}_2\bar{q}_1$ can be obtained from the $q_1\bar{q}_2 \to VHg \to \ell_1\bar{\ell}_2 g$ squared amplitude by crossing $p_2 \leftrightarrow -p_6$ and $p_1 \leftrightarrow -p_6$, respectively. Furthermore, one has to correct for an overall minus sign and change the color average from $\frac{1}{3}\times\frac{1}{3}$ to $\frac{1}{3}\times\frac{1}{8}$.

The integrations over $(n+1)$-body phase space and $dx_1\,dx_2$ are done numerically by standard Monte Carlo techniques. The kinematic invariants s_{ij} and t_{ij} are first tested for soft and collinear singularities. If an invariant for a subprocess falls in a soft or collinear region of phase space, the contribution from that subprocess is not included in the cross section.

III. RESULTS

The numerical results presented in this section have been obtained using the two-loop expression for α_s. The QCD scale $\Lambda_{\rm QCD}$ is specified for four flavors of quarks by the choice of parton distribution functions and is adjusted whenever a heavy quark threshold is crossed so that α_s is a continuous function of Q^2. The heavy quark masses were taken to be $m_b = 5$ GeV and $m_t = 150$ GeV. The standard model parameters were taken to be $M_Z = 91.173$ GeV, $M_W = 80.22$ GeV, $\alpha(M_W) = 1/128$, and $\sin^2\theta_{\rm w} = 1 - (M_W/M_Z)^2$. The soft and collinear cutoff parameters were taken to be $\delta_s = 10^{-2}$ and $\delta_c = 10^{-3}$. The parton subprocesses have been summed over u, d, c, and s quarks and the Cabibbo mixing angle has been chosen such that $\cos^2\theta_C = 0.95$. The narrow width approximation was used for the leptonically decaying weak boson and $\Gamma_W = 2.12$ GeV and $\Gamma_Z = 2.487$ GeV were used for the widths of the W and Z bosons. Except where otherwise stated, a single scale $Q^2 = M_{VH}^2$, where M_{VH}^2 is the invariant mass of the VH system, has been used for the renormalization scale μ^2 and the factorization scale M^2. The Martin-Roberts-Stirling set S0 distributions [21], which have been fit to next-to-leading order in the $\overline{\rm MS}$ scheme with $\Lambda_4 = 215$ MeV, were used for the parton distribution functions. For convenience, these distributions were also used for the leading-order (LO) calculations, although strictly speaking, one should use a leading-order parametrization of the parton distributions for LO calculations.

To study the effect of the order-α_s corrections on the leading-order processes we first consider the cross section without any cuts on the final-state particles. The relative size of the cross section is relatively insensitive to the

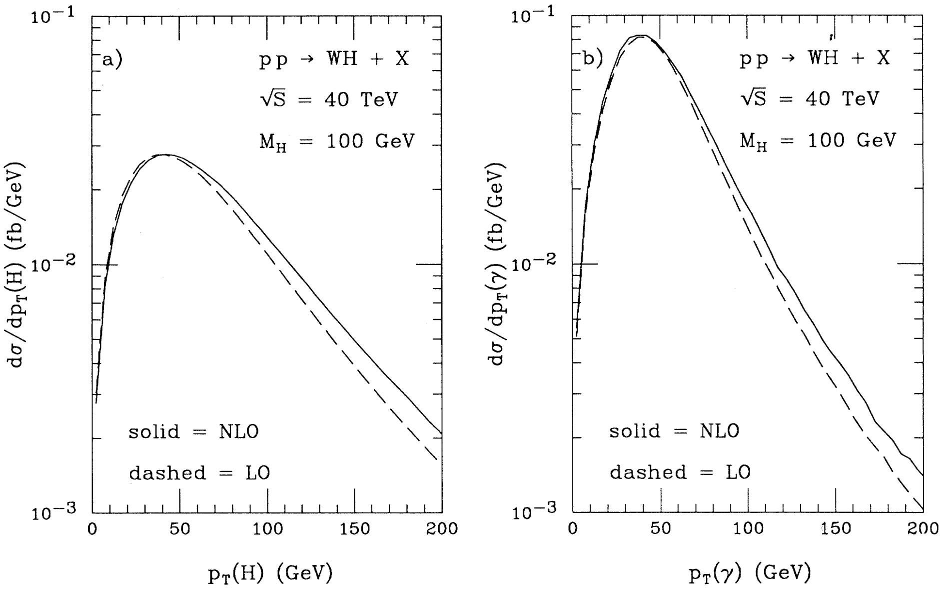

FIG. 4. Transverse momentum distribution of the Higgs boson (a) and the decay photons (b) at leading order (dashed curve) and at next-to-leading order (solid curve) for $pp \to WH + X$ at $\sqrt{s} = 40$ TeV and $M_H = 100$ GeV. Decay branching fractions $B(W \to e\nu, \mu\nu)$ and $B(H \to \gamma\gamma)$ are included.

overall center-of-mass energy $\sqrt{s}$ and to the Higgs mass (in the intermediate mass range) and so for simplicity we present only results for Superconducting Super Collider (SSC) energies and $M_H = 100$ GeV, unless otherwise stated.

Figure 4 shows the $p_T(H)$ and $p_T(\gamma)$ distributions for $pp \to WH + X$ for $M_H = 100$ GeV and $\sqrt{s} = 40$ TeV at leading order (dashed line) and with the order-α_s corrections included (solid line). Here and elsewhere, we have summed over W^+ and W^- and have included $W \to e\nu$ and $W \to \mu\nu$ decays. [Both photons have been histogrammed in the $p_T(\gamma)$ distribution.] We see from Fig. 4 that the overall correction is small and increases slowly with increasing p_T. This is illustrated more clearly in Fig. 5(a), which shows the ratio of the NLO to LO cross sections. At small $p_T(\gamma)$ values [$p_T(\gamma) \approx 50$ GeV], where the differential distribution peaks, the correction is of order 10% or less. At higher $p_T(\gamma)$ values [$p_T(\gamma) > 100$ GeV] the correction rises to between 20% and 40%. The effect of the NLO correction on the *integrated* cross

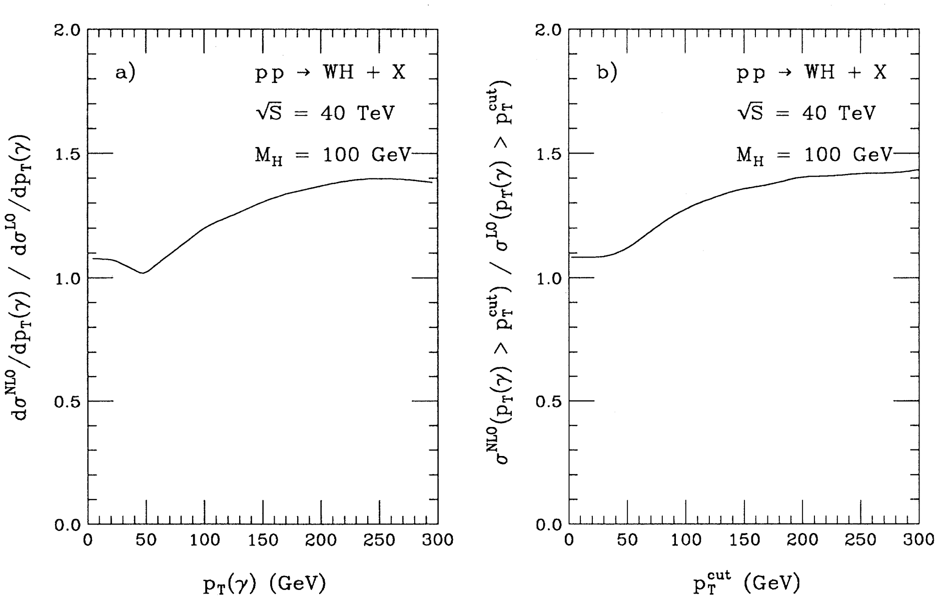

FIG. 5. The ratio of leading to next-to-leading transverse momentum distributions: (a) $[d\sigma^{\rm NLO}/dp_T(\gamma)]/[d\sigma^{\rm LO}/dp_T(\gamma)]$ and (b) $\sigma^{\rm NLO}(p_T(\gamma) > p_T^{\rm cut})/\sigma^{\rm LO}(p_T(\gamma) > p_T^{\rm cut})$ as a function of $p_T(\gamma)$ and $p_T^{\rm cut}$, respectively.

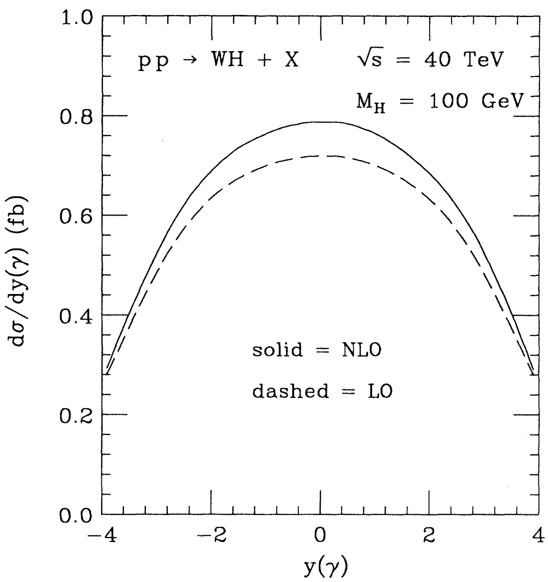

FIG. 6. Photon rapidity distribution (in the laboratory frame) at leading order (dashed curve) and at next-to-leading order (solid curve) for $pp \to WH + X$ at $\sqrt{s} = 40$ TeV and $M_H = 100$ GeV. Decay branching fractions $B(W \to e\nu, \mu\nu)$ and $B(H \to \gamma\gamma)$ are included.

section, $\sigma(p_T(\gamma) > p_T^{\rm cut})$, is shown in Fig. 5(b). Since the experimental threshold for isolated photon detection is likely to be somewhere in the $0 - 50$-GeV range, we see that the NLO correction increases the overall rate by approximately 10%. Note that the value of the NLO/LO ratio at $p_T^{\rm cut} = 0$ GeV is simply the correction to the total WH cross section and our result there is in agreement with the total cross-section calculation of Ref. [9]. Further evidence of the uniform effect of the NLO correction on the cross section is provided by Fig. 6, which shows the photon rapidity distribution at LO (dashed curve) and at NLO (solid curve) with no $p_T(\gamma)$ cut. The correction is approximately 10% over all the experimentally relevant rapidity range. The rapidity distributions of the Higgs boson and of the lepton from the W decay show very similar behavior.

We next study the effect of the NLO correction on the cross section in the presence of cuts on the final-state particles. In the present context, where our primary interest is in the relative size of the NLO correction, it is sufficient to choose cuts that approximately match the likely experimental situation. Thus, the following "representative" acceptance cuts have been applied to the cross sections calculated below:

$$p_T(\gamma) > 20 \text{ GeV}\,, \quad p_T(\ell) > 20 \text{ GeV}\,, \quad \not{p}_T > 20 \text{ GeV}\,, \qquad (24)$$

$$|y(\gamma)| < 2.5\,, \quad |y(\ell)| < 2.5\,.$$

The symbol $\not{p}_T$ denotes the missing transverse momentum carried off by the neutrino.

Figure 7 shows the $p_T(H)$ and $p_T(\gamma)$ distributions with the above cuts imposed. The NLO (solid) and LO (dashed) curves exhibit behavior similar to the no-cut distributions discussed earlier, i.e., the correction is small at small p_T and increases with p_T as the cross section falls rapidly to zero.

The final quantity that we study is the energy asymmetry of the photons from the Higgs-boson decay. The energy asymmetry is conveniently parametrized by the

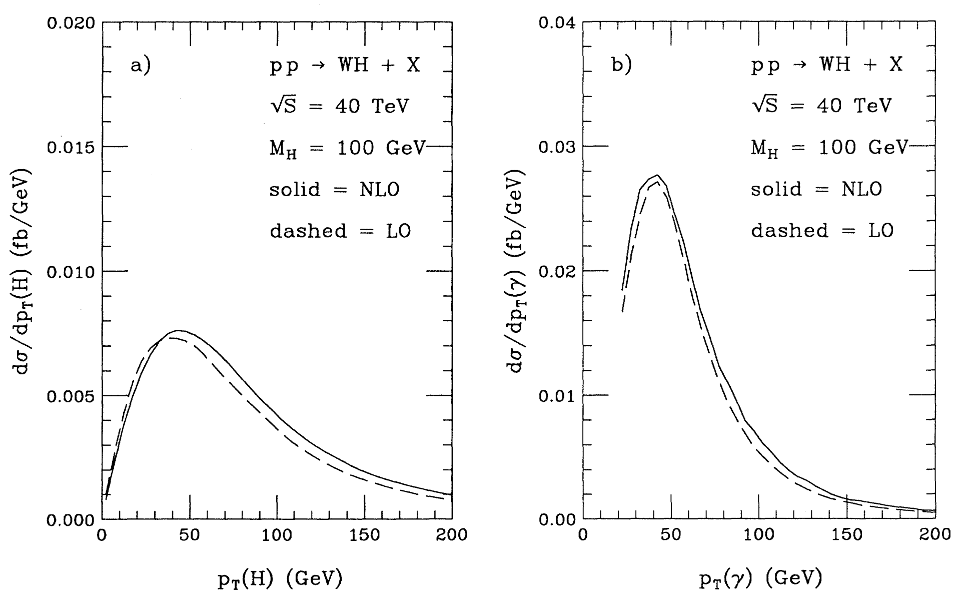

FIG. 7. Transverse momentum distribution of the Higgs boson (a) and the decay photons (b) at leading order (dashed curve) and at next-to-leading order (solid curve) for $pp \to WH + X$ at $\sqrt{s} = 40$ TeV, $M_H = 100$ GeV, and final-state cuts as described in Eq. (24). Decay branching fractions $B(W \to e\nu, \mu\nu)$ and $B(H \to \gamma\gamma)$ are included.

variable

$$x_E = \frac{|E_{\gamma_1} - E_{\gamma_2}|}{E_{\gamma_1} + E_{\gamma_2}} . \quad (25)$$

Figure 8 shows $d\sigma/dx_E$ at leading (dashed curve) and next-to-leading (solid curve) order. The correction is again uniform over the whole range. Note that the distributions peak at small x_E, indicating a preference for the photons to share the energy of the parent Higgs boson. It is interesting to contrast this behavior with that of the principal irreducible background, $pp \to W\gamma\gamma + X$, where for a fixed $M_{\gamma\gamma}$ there is a preference for one of the photons to be soft, reflecting the presence of infrared singularities in the matrix element. Thus Fig. 8 also shows the x_E distribution for the $W\gamma\gamma$ background, calculated with the same cuts as for the signal and selecting the range $M_{\gamma\gamma} = M_H \pm 10$ GeV. In the absence of any cuts the background distribution would be singular as $x_E \to 1$, but this is regulated by the p_T cut on the photons. Unfortunately, after imposing cuts, the signal and background distributions end up looking rather similar, with only a slight preference for the signal to be more peaked at small x_E.

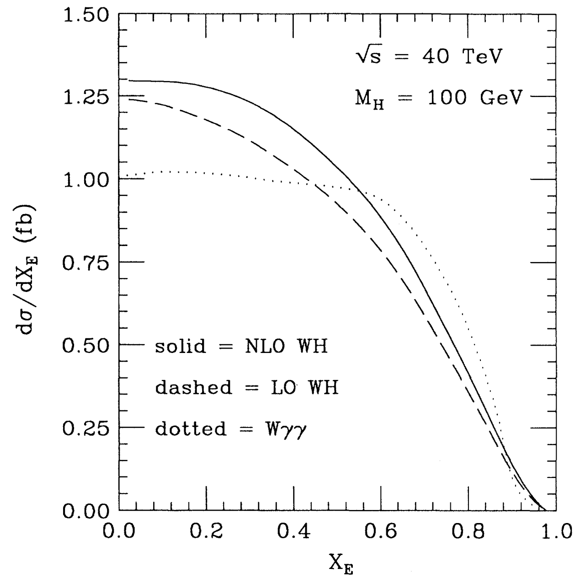

FIG. 8. Distribution in the photon energy asymmetry variable x_E defined in Eq. (25), for the WH signal at LO (dashed curve) and NLO (solid curve) and for the $W\gamma\gamma$ background (dotted curve) calculated with $M_{\gamma\gamma} = M_H \pm 10$ GeV for $M_H = 100$ GeV, $\sqrt{s} = 40$ TeV, and final-state cuts as described in Eq. (24).

IV. SUMMARY

We have studied the order-α_s perturbative QCD corrections to the fully differential Higgs boson production process $pp \to V(\to \ell_1\bar{\ell}_2)H(\to \gamma\gamma) + X$. This allows a proper calculation of the effect of the QCD correction in the presence of cuts on the final-state particles, as needed to simulate this process in a detector situation. When the final-state particles are integrated over all of phase space, we confirm the result of Ref. [9] that the total cross section correction at CERN Large Hadron Collider (LHC) and Supercondcuting Super Collider energies for the intermediate-mass Higgs boson is of order +10%. We find that this correction is approximately uniform over the phase space of the final-state particles. Only for large values of the Higgs boson (and photon) transverse momentum does the correction increase to nearly 50%, but of course in this region there are very few events. The conclusion is that the leading-order cross section with an overall rescaling is a reasonable approximation to the fully corrected cross section. Put another way, the order-α_s correction has no dramatic structure with respect to the final-state momenta, which would have enabled the acceptance cuts to be optimized to further improve the signal-to-background ratio.

We have concentrated on the WH signal, although the formalism for computing the order-α_s correction applies equally well to ZH production. When the leptonic and photonic decay branching ratios are included, this latter process unfortunately gives too few events to be experimentally relevant, except perhaps if very high luminosities can be achieved [22]. (The ZH total cross section with branching fractions is a factor of 5 smaller than the corresponding WH cross sections discussed here.) Our modest perturbative correction has not improved this situation.

Note added. After completing this work we learned of a similar calculation by Baer, Bailey, and Owens [23]. We have confirmed that our results agree with their results.

ACKNOWLEDGMENTS

J.O. wishes to thank T. Han for useful discussions and the UK Science and Engineering Research Council for support. J.O. also wishes to thank Fermilab and Argonne National Laboratory for hospitality while this work was being completed.

[1] S. L. Glashow, D. V. Nanopolous, and A. Yildiz, Phys. Rev. D **18**, 1724 (1978).

[2] R. Kleiss, Z. Kunszt, and W. J. Stirling, Phys. Lett. B **253**, 269 (1991).

[3] J. Gunion, G. Kane, and J. Wudka, Nucl. Phys. **B299**, 231 (1988).

[4] SDC Collaboration, M. Mangano, Report No. SSC-SDC-90-00113 (unpublished).

[5] J. Gunion and G. Kane, University of California–Davis, Report No. UCD-91-0010 (unpublished); also in *Research Directions for the Decade*, Proceedings of the 1990 DPF Summer Study on High Energy Physics, Snowmass, Col-

orado, 1990, edited by E. L. Berger (World Scientific, Singapore, 1991).

[6] Z. Kunszt and W. J. Stirling, in *Proceedings of the ECFA Large Hadron Collider Workshop*, Aachen, Germany, 1990, edited by G. Jarlskog and D. Rein (CERN Report No. 90-10, Geneva, Switzerland, 1990), Vol. II, p. 428.

[7] C. Seez *et al.*, in *Proceedings of the ECFA Large Hadron Collider Workshop* [6], Vol. II, p. 474.

[8] J. F. Gunion, H. E. Haber, G. L. Kane, and S. Dawson, *The Higgs Hunter's Guide* (Addison-Wesley, Menlo Park, CA, 1990).

[9] T. Han and S. Willenbrock, Phys. Lett. B **273**, 167 (1991).

[10] J. Ohnemus and J. F. Owens, Phys. Rev. D **43**, 3626 (1991).

[11] J. Ohnemus, Phys. Rev. D **44**, 1403 (1991).

[12] J. Ohnemus, Phys. Rev. D **44**, 3477 (1991).

[13] B. Bailey, J. Ohnemus, and J. F. Owens, Phys. Rev. D **46**, 2018 (1992).

[14] J. Ohnemus, Phys. Rev. D **47**, 940 (1993).

[15] H. Baer, J. Ohnemus, and J. F. Owens, Phys. Rev. D **42**, 61 (1990); Phys. Lett. B **234**, 127 (1990).

[16] H. Baer, J. Ohnemus, and J. F. Owens, Phys. Rev. D **40**, 2844 (1989).

[17] L. Bergmann, Ph.D. dissertation, Florida State University, Report No. FSU-HEP-890215, 1989 (unpublished).

[18] H. Baer and M. H. Reno, Phys. Rev. D **43**, 2892 (1991).

[19] G. 't Hooft and M. Veltman, Nucl. Phys. **B44**, 189 (1972).

[20] W. A. Bardeen, A. J. Buras, D. W. Duke, and T. Muta, Phys. Rev. D **18**, 3998 (1978).

[21] A. D. Martin, W. J. Stirling, and R. G. Roberts, Phys. Rev. D **47**, 867 (1993).

[22] A. Grau, T. Han, and G. Pancheri, in *Proceedings of the ECFA Large Hadron Collider Workshop* [6], Vol. II, p. 488.

[23] H. Baer, B. Bailey, and J. F. Owens, following paper, Phys. Rev. D **47**, 2730 (1993).